

# Minimizing the Induced Fields in MRI Occupational Workers by Lowering the Imager

A. TRAKIC, H. WANG, F. LIU, H.S. LOPEZ, E. WEBER, S. CROZIER

*School of Information Technology and Electric Engineering, The University of Queensland, Brisbane, QLD 4072, Australia*

**ABSTRACT:** In magnetic resonance imaging (MRI), healthcare workers can be exposed to strong static and time-varying magnetic fields outside the imager. Body motion through the large, spatially nonuniform static magnetic field generated by the main magnet and exposure to low-frequency magnetic fields from pulsed gradient coils can lead to the stimulation of electric fields in the body. Tissue of the central and peripheral nervous system (CPNS) in the head and torso is particularly susceptible. To protect occupational workers, the member states of the European Union are required to incorporate the physical agents directive (PAD) 2004/40/EC into their legislation, which could restrict the use of MRI in some cases. This article reports a rather simple and general method/solution that can notably reduce the head/trunk exposure of MRI operators to both static and (low-frequency) time-dependant magnetic fields in MRI. It is numerically shown that the upper body CPNS exposure can be reduced by factors of up to 50 or more, when the MRI machine is simply lowered by 1 m in height relative to the ground floor. The proposed approach can lead to significantly reduced in situ electric fields/current in the upper body and thus allow faster worker motions around the lowered imager. © 2008 Wiley Periodicals, Inc. Concepts Magn Reson Part B (Magn Reson Engineering) 33B: 39–54, 2008

**KEY WORDS:** MRI; physical agents directive 2004/40/EC; magnetic field

## INTRODUCTION

Modern magnetic resonance imaging (MRI) exploits a wide spectrum of electromagnetic (EM) frequencies and field strengths for the rapid generation of high-resolution images (1). The fields generated by the various components of the imager interact with the patients and occupational workers in a variety of ways, leading to a range of possible effects (2, 3).

Received 15 July 2007; revised 10 September 2007; accepted 11 September 2007

Correspondence to: Stuart Crozier; E-mail: stuart@itee.uq.edu.au

Concepts in Magnetic Resonance Part B (Magnetic Resonance Engineering), Vol. 33B(1) 39–54 (2008)

Published online in Wiley InterScience (www.interscience.wiley.com). DOI 10.1002/cmr.b.20102

© 2008 Wiley Periodicals, Inc.

## On the Static Magnetic and Gradient-Pulsed Field Exposure

Strong static magnetic fields might induce notable electric fields in tissues as the MRI workers or patients are moving through the spatial three-dimensional gradients of the static magnetic field in the close proximity of the imager (4). The induced flow potentials may become physiologically significant at field strengths in excess of  $\sim 2$  T (2–5), where following physiological responses could be observed: headaches, nausea, vertigo, phosphenes (light flashes), numbness and tingling, loss of proprioception and balance, and a metallic taste in the mouth associated with the rapid head movements etc. These biological responses could be a result of synapse excitations in the central nervous system (CNS) (2–5). However, the exact mechanism(s) of interaction between the gradient of the static magnetic field

and the tissue (synapses or others) are still arguable. Further research work is essential to completely delineate the observed effects and interaction models. The Institute of Electrical and Electronics Engineers (IEEE) guideline for exposure to magnetic fields at frequencies below 1 Hz assumes biological reactions at fields above 1.5 T-peak (3). For brain tissue (in controlled environments), the IEEE guideline limits the induced electric field to 25.03 mV/m (<20 Hz).

Another safety concern in MRI is related to the human exposure to low-frequency magnetic fields generated by pulsed gradient coils at frequencies of around 1 kHz. The interaction of time-varying gradient fields and tissue can result in depolarization of voltage sensitive ion-channels/membranes and subsequent nerve excitation (6, 7). Patients who are situated inside an MRI bore and were subjected to strong time-varying magnetic fields have experienced physiological reactions that are mainly attributed to the excitation of peripheral nerves (8, 9). Peripheral nerve stimulation (PNS) can range from harmless tingling feelings in the skin, to burning sensations, and even pain. Results from a most recent study (10) indicate that fields produced by the gradient coils can lead to similar levels of electric field/current induction in healthcare workers, particularly when standing near or bending towards the gradient set entrance. Today, MRI scanners are generally constructed according to the international standard IEC 60601-2-33 to minimize the risk of PNS.

### On the EC Physical Agents Directive

The physical agents directive (PAD) 2004/40/EC of the European Parliament and of the Council on the minimum health and safety requirements regarding the exposure of workers to the risks arising from physical agents (EM fields) was introduced on the April 29, 2004 and it applies to all EM-radiating environments, including MRI (11). The EC PAD, which seeks to protect occupational workers from overexposure to EM-fields, forms an essential requirement that must be implemented into law by every member state of the European Union (EU) in the near future.

As the MRI technology moves into higher field strengths for improved resolution and contrast, the interaction of EM-fields generated by new generation scanners and occupational workers has attracted substantial attention and awareness (10). These concerns relate in particular to situations in which the medical staff is obliged to attend anxious, sedated or intubated patients during the imaging procedure, while it is

believed that limits of exposure set out in the directive may well be exceeded in the vicinity of the imager bore opening. The directive however, does not apply to patients or volunteers undergoing the MRI examination. In contrast, the MRI community has expressed concerns that the realization of the EC PAD would have severe consequences for the use, development and maintenance of MRI in medical, research, and industrial settings (12).

### The Precautionary Approach

As MRI researchers we hope that working around MRI systems is completely safe; however, there really has never been a full and well controlled MRI-based epidemiological study that measured exposures, so we must act with some caution balanced with benefit to patients. Therefore, it is important to carefully research and quantify the fields that healthcare workers are exposed to during normal practice and to adopt a level of sensible precaution.

### This Work

This comparative theoretical study involves an anatomically realistic human voxel phantom in various motions and body postures around realistic 1.5, 4, and 7 T superconducting magnets and trapezoidally switched  $x$ ,  $y$ , and  $z$ -axis gradient coils to evaluate exposure levels an occupational worker is likely to experience in routine MRI interventions. The principal assertion of this work is that increasing the (vertical) separation between the upper body and the imager central axis can lead to appreciable reduction in induced electric field/current levels in the head and trunk, which contains the tissue of CNS and other vital body organs. For instance, lowering the 1.5 T system by 1 m from its original height of 1.15 m will shift the exposure away from the head/trunk to the lower leg region, thus minimizing the in situ electric fields by factors of up to 50 and more in brain and other upper body tissues. Similarly, exposure to the switched gradient coils is notably reduced by implementing this approach. Further reduction of exposure is possible when the scanner is lowered by more than 1 m, or when the occupational worker is raised up in respect to the magnet by constructing an elevation platform around an (existing) MRI scanner. Finally, various MRI system implementations that incorporate the proposed method/solution are discussed.

Irrespective of any claims of the effect of the fields generated by an MRI system on healthcare

**Table 1 Superconducting Magnet Geometry**

B (T)	DSV Size (5 ppm) $r$ (cm) $\times$ $z$ (cm)	Length (m)	Inner Radius (m)	Outer Radius (m)	5 Gauss Shielding $r$ (m) $\times$ $z$ (m)
1.5	40 $\times$ 50	1.27	0.48	0.87	$\sim 3.6 \times 4.2$
4.0	–	2.09	0.52	1.02	$\sim 4 \times 6$
7.0	52 $\times$ 52	2.60	0.49	0.77	$\sim 14 \times 18$

–, not available.

workers, and irrespective of any present or future regulatory limit values, this work merely presents a possible and simple way of substantially minimizing the upper body exposure of workers and patients around existing and future MRI systems.

## MATERIALS AND METHODS

### Computational Resources

**Main Magnets.** To evaluate the exposure of an MRI operator to different magnetic field strengths/spatial profiles, this work considers three realistic symmetric superconducting magnets: 1.5 T Infinion (actively shielded) (13), 4 T Siemens (actively shielded), and 7 T in-house developed research magnet (unshielded). Table 1 details the geometries of the three magnets.

Figure 1 illustrates a homogeneous static magnetic field in the working volume and the rapid field drop off near the magnet ends, where during the body motion largest electric field induction is most likely to occur.

It is assumed that the superconducting coils of the 1.5 and 4 T magnets are embedded in a cryostat vessel, which extends the magnets by 0.1 m both radi-

ally and axially. The cryostat vessel of the 7 T imager, however, broadens the magnet by 0.1 m axially and 0.25 m radially.

**Gradient Coils.** For this numerical investigation, actively-shielded, whole-body, symmetric  $x$ ,  $y$ , and  $z$ - gradient coils were in-house designed (14, 15). The three coils have approximately the same length of  $\sim 1.4$  m, while the six coil layers (primary and secondary) are allocated to different radii assuming a layer thickness (including former, etc) of 5 mm. The axial length of  $\sim 1.4$  m is chosen so that the gradient coils would fit inside the available geometry of the 1.5 T magnet (see Table 1) or larger scanners. Table 2 lists some important gradient coil parameters.

It was assumed that each coil generates normalized gradient field strength of 1 mT/m in the working volume so that the simulation results can be linearly extrapolated to other field strengths of interest. It was also assumed that the gradient coils are pulsed trapezoidally at a frequency of 1 kHz with a rise time of 100  $\mu$ s. Figure 2 illustrates the total magnetic field profiles generated by the gradient coils. From the field distributions we note a rapid drop in the magnetic flux at the coil ends, which implies that these are the most likely positions to induce notable fields in the body.

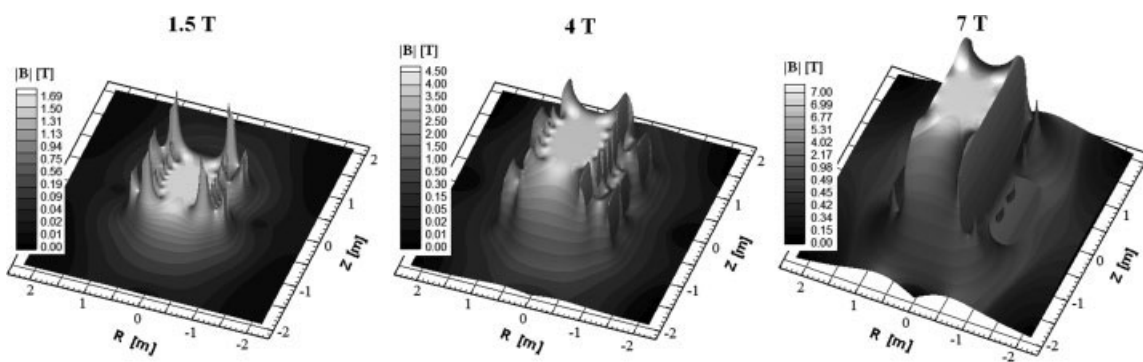


**Figure 1** Spatial profile of the total magnetic flux of the three magnets.

**Table 2 Geometrical Properties of Gradient Coils**

Parameter	x-Gradient	y-Gradient	z-Gradient
1st layer-Z (m)	1.18	1.20	1.29
2nd layer-Z (m)	1.37	1.40	1.40
1st layer-R (m)	0.31	0.32	0.33
2nd layer-R (m)	0.36	0.37	0.39
DSV: $r$ (m)			
$\times z$ (m)	$0.42 \times 0.42$	$0.42 \times 0.42$	$0.50 \times 0.56$

$Z$  denotes axial length and  $R$  denotes the radius of the primary and secondary gradient coil layers. The DSV size is given as the region where the gradient field is uniform to 5% peak-peak and is expressed as diameter by length in meters.

**Body Model.** A heterogeneous whole-body male voxel phantom BROOK (16) was used to accurately model the exposure of an occupational worker to fields produced by the main magnet and gradient coils. With some 40 body tissues identified in the

model, each voxel is assigned a measured conductivity value (17, 18) corresponding to its dominant tissue type and appropriate to the frequency of interest. The dimensions of the digital model were  $74 \times 43 \times 235$  voxels along the  $x$ ,  $z$ , and  $y$  Cartesian axis respectively. This implies a voxel resolution of roughly 8 mm, which is adequate in demonstrating the principal idea of this study.

## Computational Method

This work considers a spatially distributed time-varying magnetic flux density that arises directly from a trapezoidally oscillating current in the gradient coil(s) and/or as a conducting object, in this case human body, is moving through a spatially nonuniform magnetic field generated by the main superconducting magnet. At such low-frequencies, quasi-static assump-

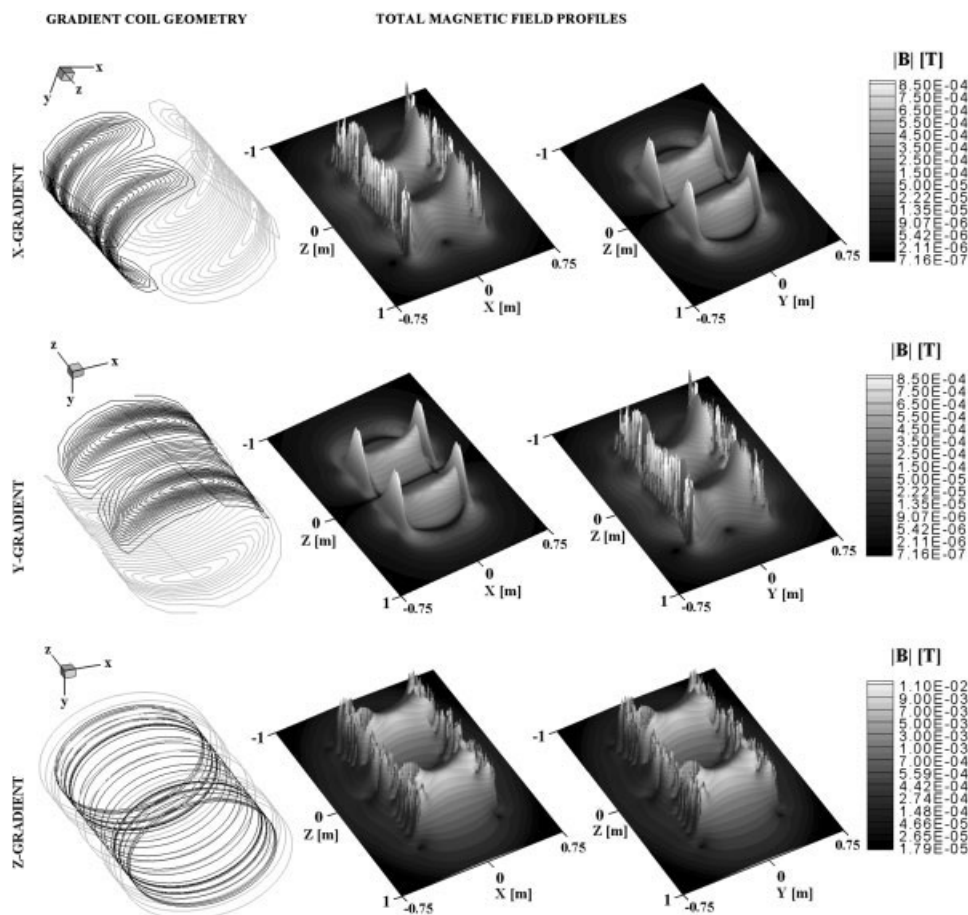


**Figure 2** Left column: three-dimensional plot of transverse and longitudinal gradient coil geometry (for transverse coils only one primary and one secondary layer is illustrated, while all coil loops are plotted for the longitudinal gradient coil). The primary and secondary windings are indicated in black and gray respectively. Middle and right column:  $x$ - $z$  and  $y$ - $z$  profiles of the total magnetic flux density generated by the three gradient coils.

tion applies and the computation of the induced electric fields was accomplished with the quasi-static finite-difference (QSFD) scheme (19). The total electric field inside the biological sample can be split into primary field  $E_1$  and secondary field  $E_2$ , according to:

$$E = E_1 + E_2, \text{ where } E_1 = -\frac{\partial A}{\partial t} \text{ and } E_2 = -\nabla\Phi \quad [1]$$

Here  $A$  and  $\Phi$  are the vector magnetic and scalar electric potential respectively.

**Computation of  $E_1$  Due to Main Magnet.** In two-dimensional axial-symmetric cylindrical coordinates, the vector magnetic potential components due to the main superconducting magnet can be expressed as:

$$A_\theta(r, z) = \sum_{m=1}^M \frac{\mu J_0(m)}{2\pi} \int_{z^S=z_1(m)}^{z_2(m)} \int_{r^S=R_1(m)}^{R_2(m)} \frac{\cos\theta d\theta}{\sqrt{(r^S)^2 + r^2 - 2r^S r \cos\theta + (z^S - z)^2}} dr^S dz^S \quad [2]$$

$$A_r(r, z) = A_z(r, z) = 0$$

In Eq. [2],  $m = 1, 2, \dots, M$  denotes the number of the thick circular solenoids,  $\mu$  is the permeability of the medium,  $J_0$  is the current density within the coil  $m$  [in  $\text{Am}^{-2}$ ]; the primed and un-primed cylindrical coordinate variables (i.e.  $r^S, z^S$ , and  $r, z$ ) refer to the source points within the solenoid and to the field points inside the body model, respectively. For each solenoid  $m$ ,  $R_1(m)$  and  $R_2(m)$  are the inner and outer radii, while  $z_1(m)$  and  $z_2(m)$  are the coil starting and ending positions in the  $z$ -direction. The inner integral in Eq. [2] can be evaluated with complete elliptic integrals (20). The vector potentials in Eq. [2] are converted from two-dimensional cylindrical to three-dimensional Cartesian coordinates using the following unit vector matrix transform:

$$\begin{bmatrix} a_x \\ a_y \\ a_z \end{bmatrix} = \begin{bmatrix} \cos\theta & -\sin\theta & 0 \\ \sin\theta & \cos\theta & 0 \\ 0 & 0 & 1 \end{bmatrix} \begin{bmatrix} a_r \\ a_\theta \\ a_z \end{bmatrix} \quad [3]$$

Then, the primary electric field  $E_1$  is expressed by the negative difference (i.e.  $-dA$ ) of the vector potentials of two neighbouring voxels divided by the time difference  $dt = h/v_\gamma$ , where  $\gamma$  is the direction of motion in Cartesian coordinates,  $h$  is the voxel size in the direction of motion in meters, and  $v$  is the magnitude of body velocity in meters per second.

The spatial precision of the displacement is therefore restricted to the cell size. We note that this formulation supports multi-directional translation using vector analyses of velocity.

**Computation of  $E_1$  Due to Gradient Coil(s).** According to the International Commission for Nonionizing Radiation Protection (ICNIRP) guideline, to assess exposure thresholds, Fourier harmonic decomposition of the pulse sequence needs to be performed. For trapezoidally pulsed gradient current the Fourier series is given by:

$$F(t) = \sum_{n=1}^{\infty} \underbrace{\frac{4I \sin((2n-1)\omega\tau)}{(2n-1)^2 \omega\pi\tau}}_{C_n} \sin((2n-1)\omega t) \quad [4]$$

where  $I$  is the amplitude of the gradient coil current in (Amps),  $t$  is transient time in (s),  $\tau$  is rise-time in (s),  $\omega$  is the angular frequency in [ $\text{rad} \times \text{s}^{-1}$ ] and  $n$  is the order of the Fourier harmonic. Then, for each Fourier harmonic  $n$ , the vector potential  $A$ , due to the segmented gradient coil(s) can be evaluated via the usual Biot-Savart method (10, 19). At least  $n = 7$  Fourier harmonics were employed to synthesize the trapezoidal gradient waveform. On the basis of this decomposition, the induced electric field components are calculated at each frequency and summed accordingly.

**Computation of  $E_2$  Due to Charge Accumulation.** On the basis of the implementation of the quasi-static finite difference scheme (QSFD) (19, 21, 22), the computation of the electric fields is given by the governing surface integral equation:

$$\int_S \left( \sigma \frac{\partial A}{\partial t} \right) \cdot dS = \int_S (\sigma \nabla \Phi) \cdot dS \quad [5]$$

where  $S$  represents the surface of the integral region. The governing Eq. [5] is subject to a boundary condition of the Neumann type:

$$\frac{\partial \Phi}{\partial n} = \hat{n} \cdot \left( -\frac{\partial A}{\partial t} \right) \quad [6]$$

which indicates that the normal component of the induced electric field on the tissue-air boundary is zero inside the body. To calculate the scalar potential  $\Phi$ , we divide the computational space into a large number of cubic cells and then Eq. [5] is approximated for each elementary cell. After discretization

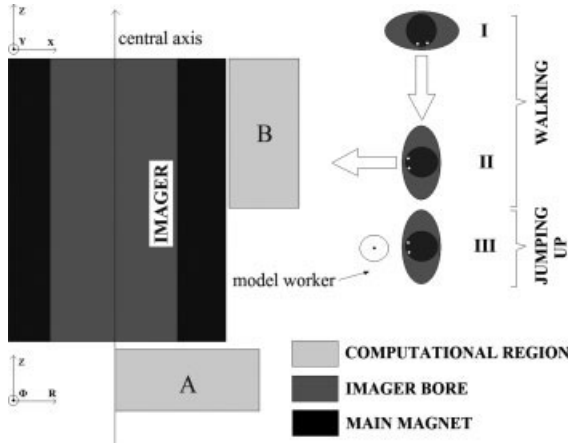


**Figure 3** Top view illustration of three assumed body motions in front (position A) and at the side (position B) of the superconducting magnet of interest (1.5T, 4T, and 7T); for detailed information on model worker position near the magnet, the reader is referred to Table 3.

and rearrangement, the scalar potential for cell  $(i, j, k)$  can be expressed as:

$$\Phi_{i,j,k} = \frac{\Xi - f(A)h}{\sum_{q=0}^1 (\sigma_{i+q,j,k}^a + \sigma_{i,j+q,k}^a + \sigma_{i,j,k+q}^a)}$$

$$\Xi = \sum_{q=0}^1 \left( \Phi_{i+q,j,k} \sigma_{i+q,j,k}^a + \Phi_{i,j+q,k} \sigma_{i,j+q,k}^a + \Phi_{i,j,k+q} \sigma_{i,j,k+q}^a \right) \quad [7]$$

$$f(A) = \sum_{q=0}^1 \left[ \begin{aligned} & \left( \sigma_{(i+q,j,k)}^a \frac{\partial A}{\partial r(i+q,j,k)} \right) \cdot s_x^q + \\ & \left( \sigma_{(i,j+q,k)}^a \frac{\partial A}{\partial r(i,j+q,k)} \right) \cdot s_y^q + \\ & \left( \sigma_{(i,j,k+q)}^a \frac{\partial A}{\partial r(i,j,k+q)} \right) \cdot s_z^q \end{aligned} \right]$$

in which subscripts  $i, j,$  and  $k$  indicate the cell indices, subscript  $q$  indicates two faces (0 or 1) in  $x, y, z$  directions, respectively,  $s$  is the unit vector normal to the cell faces,  $h$  is the cell size and  $\sigma^a$  is the local harmonic averaged conductivity. The governing Eq. [7] in finite-difference form can be solved using an iterative technique such as the successive over relaxation (SOR) algorithm (20) with the advantage of rapid convergence. After the scalar potential has been calculated, the electric field components can be found using Eq. [1].

### Model Setup

**Worker Exposure to Fields Produced by the Main Magnet.** In modeling the exposure of a moving

worker to static magnetic field produced by each of the three main magnets, three different motion actions were assumed:

Motion I – walking from the positive towards the negative  $z$ -axis.

Motion II – walking from the positive towards the negative  $x$ -axis ( $r$ -axis).

Motion III – jumping upwards while facing the negative direction of the  $x$ -axis ( $r$ -axis).

For every combination of worker motion and main magnet, we evaluate the exposure at position A and B as indicated in Fig. 3. Placement of the model worker that is undergoing a motion action in domain A is based on peak exposures that were determined in the recent study (10), whereas placements in domain B were chosen according to conceptual assessment of strong field gradients in that region. Table 3 details all designated worker positions where exposures have been evaluated. All motion velocities have been normalized to  $1 \text{ m s}^{-1}$  and assumed to be constant throughout the voxel phantom. In that way the gathered results can be linearly extrapolated to other velocities of interest. In an attempt to mimic realistic human movement, suitable velocities can be assigned to different body parts.

At first, the three superconducting magnets are placed 1.15 m above ground (setup I) relative to their central cylinder axis ( $r = 0$ ), as this is the vertical elevation common to most clinical MRI scanners [see Fig. 4(a)]. At this elevation all exposures as detailed in Table 3 were carried out. Then the magnet was lowered by 1 m to a vertical elevation of 0.15 m (setup II). This implies that the table which brings the patient inside the magnet bore lies directly on the ground floor as shown in Fig. 4(b).

Exposures based on Table 3 were then repeated for the scanner elevation of 0.15 m.

**Worker Exposure to Fields Produced by the Gradient Coils.** All three symmetric gradient coils create the same magnetic field profiles and strengths at both

**Table 3** Worker Positions Around Main Magnet

Motion Type	Pos*	1.5 T		4 T		7 T	
		R (m)	Z (m)	R (m)	Z (m)	R (m)	Z (m)
I	A	0.30	-0.90	0.30	-1.30	0.30	-1.55
	B	1.30	0.40	1.45	0.60	1.20	0.80
II	A	0.50	-1.00	0.20	-1.40	0.20	-1.70
	B	1.20	0.40	1.35	0.60	1.10	0.80
III	A	0.20	-1.00	0.20	-1.40	0.20	-1.70
	B	1.20	0.40	1.35	0.60	1.10	0.80

Pos\*, position of the model around the magnet of interest; A, in front of main magnet; B, at one side of main magnet.

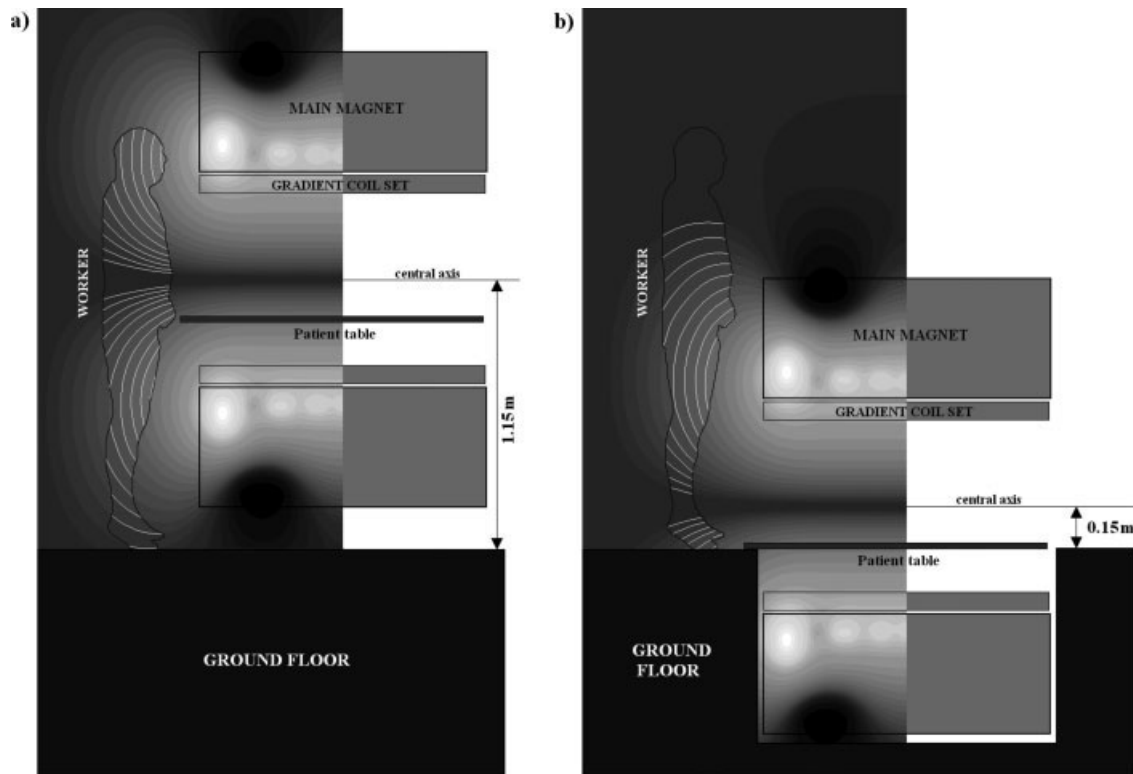


**Figure 4** The two considered imager elevations: (a) setup I, where the MRI system is 1.15 m above the ground; (b) setup II, where the MRI system is lowered by 1 m to a new height of only 0.15 m relative to the ground floor. More importantly the figure illustrates the profile of the vector magnetic potential produced by the 1.5 T superconducting magnet and the way vector potential lines cross the body model for setup I and II.

ends of the coil. The walls of the cryostat vessel/thermal radiation walls, shield the superconducting magnets inside the helium tank by attenuating the residual fields of the pulsed gradients. Therefore the magnetic fields to the sides of the MRI scanner are quite small in magnitude, while the fields near the coil ends represent the major risk areas due to worker access. At first, the stationary model worker is positioned at  $r = 0$  m to face the gradient set end, while the frontal body surface is 1 cm away from the imager end, as Fig. 5(a) shows. This particular situation can occur during the installation and testing of the MRI system in industrial settings, however, because of the presence of the patient table in clinical applications, the worker might not be able to reach this particular location. In the second scenario, the patient table is considered, and the model worker is assumed to face the table at  $r = 0.31$  m (relative to front body surface) while the right shoulder is 1 cm away from the end of the gradient set [see Fig. 5(b)]. In the third scenario, as Fig. 5(c) illustrates, the body model is positioned just right to the patient table while facing the gradient set (the worker is assumed

to be 1 cm away from both the patient table and the gradient set end). The patient table was assumed to be 0.5 m in width and  $\sim 2$  m in length.

All three gradient coils are pulsed simultaneously (i.e., oblique imaging) as this would represent major exposure to the worker. Similar to static field exposure study, all designated gradient pulsed field calculations were performed for scanner elevations of 1.15 m (setup I) and 0.15 m (setup II). Then, the simulations results of two gradient set elevations were assessed and compared.

## RESULTS

### Worker Exposure to Fields Produced by the Main Magnet

The simulations converge in about 4,000 iterations and the typical computation time is around 3 min on a dual XEON 3.6 GHz/4 GB RAM PC platform. Figures 6 and 7 illustrate the selected electric field profiles in coronal and sagittal slices of the voxel phantom induced during the assumed body motions

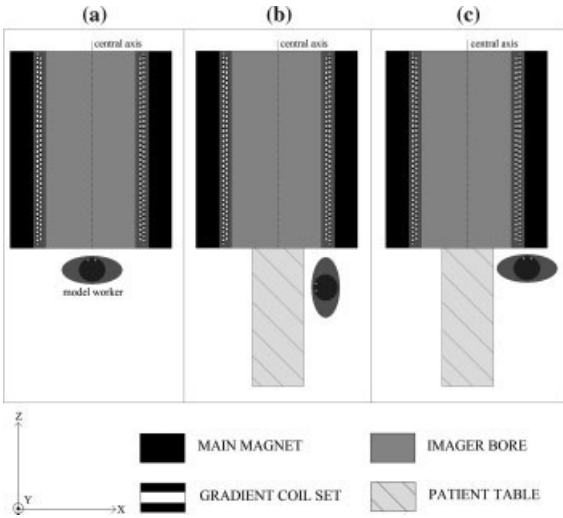


**Figure 5** Assumed model worker positions near the gradient coil set: (a) the model worker (MRI technician) is centrally in front of the gradient set (i.e., 1 cm away from the gradient set end), in which case the patient table was not considered; (b) the body model (radiologist) is facing the patient table while the right shoulder is 1 cm away from the gradient set end; (c) the body model is facing the gradient set while standing just right to the patient table. In (b) and (c) the patient table is assumed to be 50 cm in width.

around the three designated superconducting magnets. More importantly, Figs. 6 and 7 compare the levels of field induction in the whole body for mag-

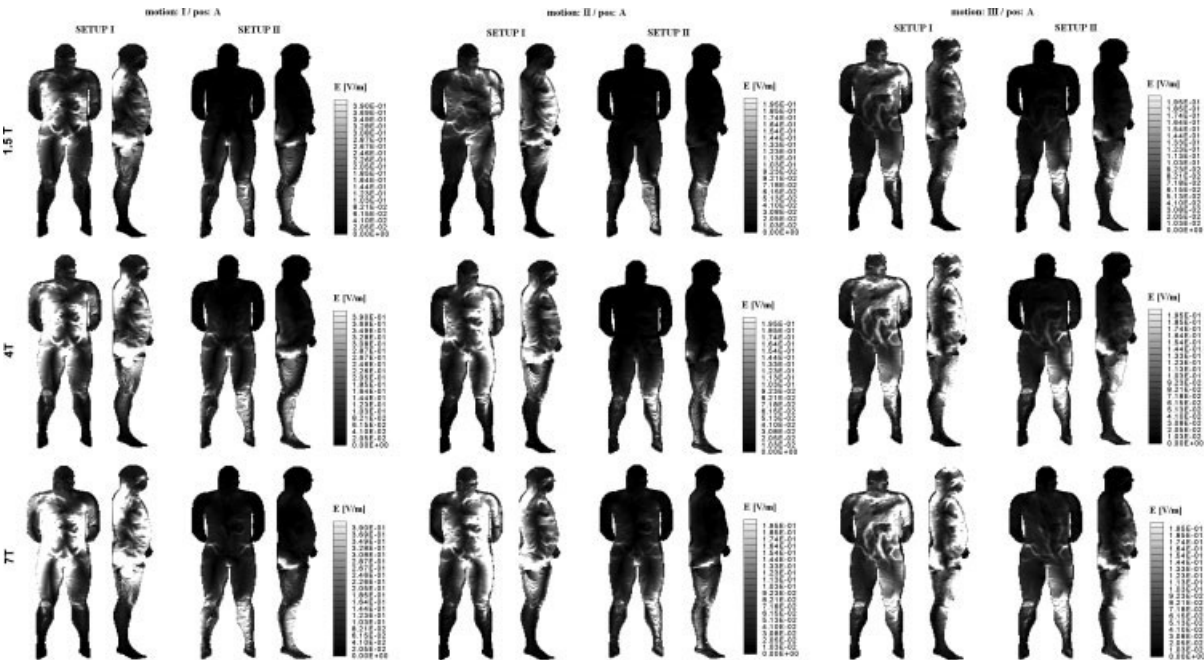
net elevations of 1.15 m (setup I) and 0.15 m (setup II). Figure 8 compares the maximum and average electric field within each axial slice versus height of the model worker between setup I and II. The line graphs are based on results of motion I around all three superconducting magnets at position A (see Table 3).

Table 4 compares the maximum and average induced electric field for tissues of the CNS, while Table 5 details the factor of exposure reduction between setup I and II.

Figure 9 illustrates the average electric field for CNS tissues as a function of the magnet height above ground floor. Clearly, as the magnet height decreases, the CNS exposure decreases.

**Worker Exposure to Fields Produced by the Gradient Coils**

The convergence performance of body exposure to gradient fields was very similar to that of the static field study. Figure 10 compares the induced electric fields in coronal and sagittal planes of the body between setup I and II for the three designated postures near the imager end (see Fig. 5). Also illustrated are the electric field averages for each axial slice versus body height. These electric field induction results are based on simultaneous trapezoidal pulsing (1 kHz/ 100  $\mu$ s rise time) of all three gradient coils at a normalized central field strength of 1 mT/m.



**Figure 6** Coronal and sagittal plots of electric field distributions in the model worker induced during motion I–III at position A near each superconducting magnet.

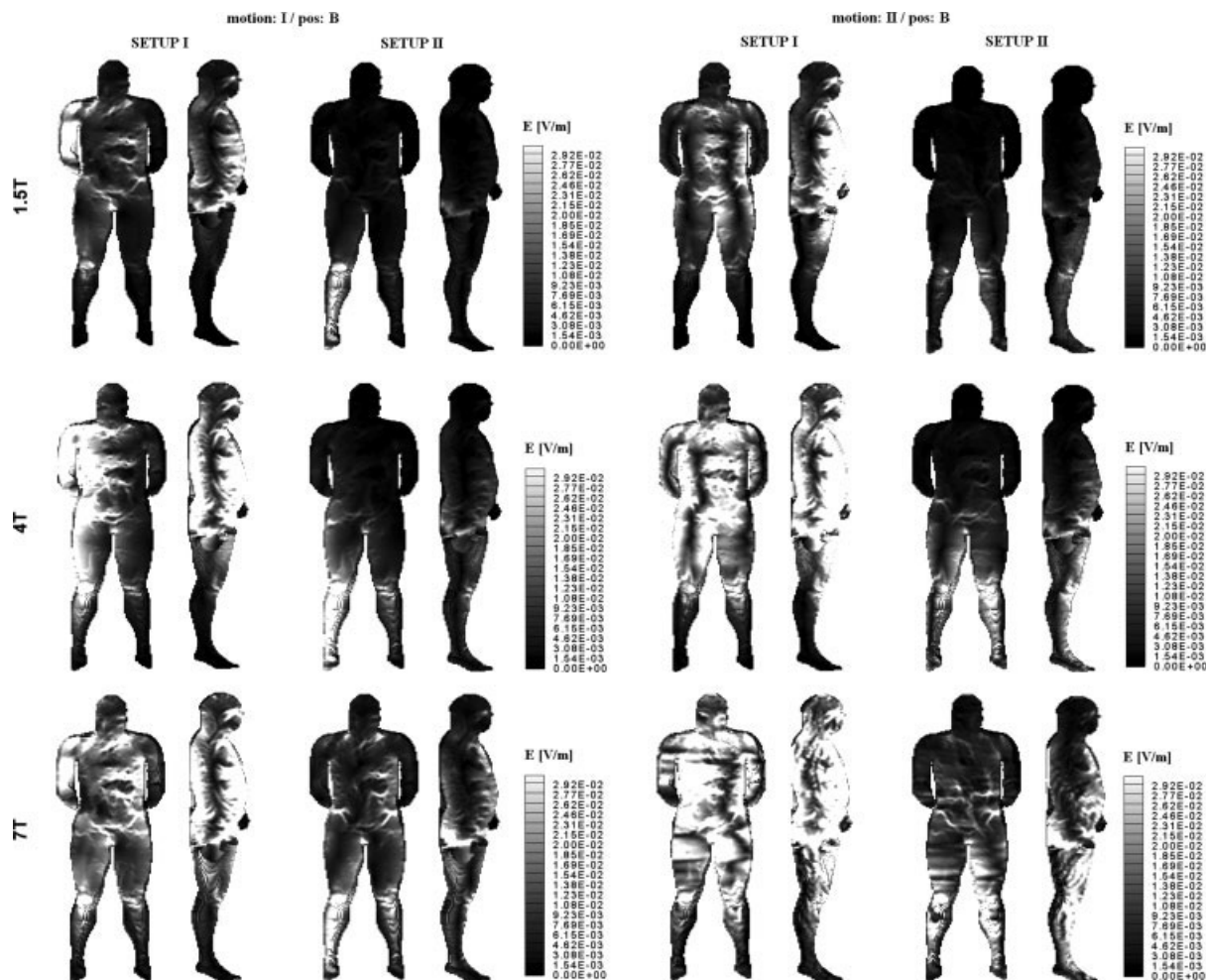


**Figure 7** Coronal and sagittal plots of electric field distributions in the model worker induced during motion I–II at position B near each superconducting magnet.

By extrapolating the results to 35 mT/m as currently used in clinic, we note that the levels of induced electric fields are in the same order of magnitude as those induced in patients during imaging and therefore should not be ignored. A gradient rise-time of 100  $\mu$ s was assumed, while typical maximum rise-times in clinical practice are around 200–250  $\mu$ s. According to [4], to increase the rise-time from 100 to 250  $\mu$ s while keeping all other parameters same, one should scale down all electric field values by a factor of  $\sim 1.84$ .

## DISCUSSION

### On the Worker Exposure to Fields Produced by the Main Magnet

The level of exposure is proportional to the velocity of body motion and the spatial gradient of the static

magnetic field produced by the main cylindrical magnet. In general, strongest bending of magnetic flux lines (spatial gradient) takes place between two or more superconducting coils where currents are flowing in opposite directions and near the bore edges at each magnet end. The standard magnet elevation (i.e.,  $\sim 1.15$  m) specified by the manufacturer is such that the region of the bore entrance, where strong spatial (static) magnetic field gradients exist, is at the height level of the middle body section of the person undergoing the motion near the imager. Considering the large bore diameter of the superconducting magnet (i.e.,  $\sim 1$  m), one can expect a large region of the body below and above the centre of circular bore to be spanned by the strong static magnetic field gradients (see Fig. 4). Subsequently, as the worker is moving near the magnet end, notable fields can be induced in the upper, mid as well as lower body region (i.e. head, neck, chest, abdominals, upper legs, and arms)

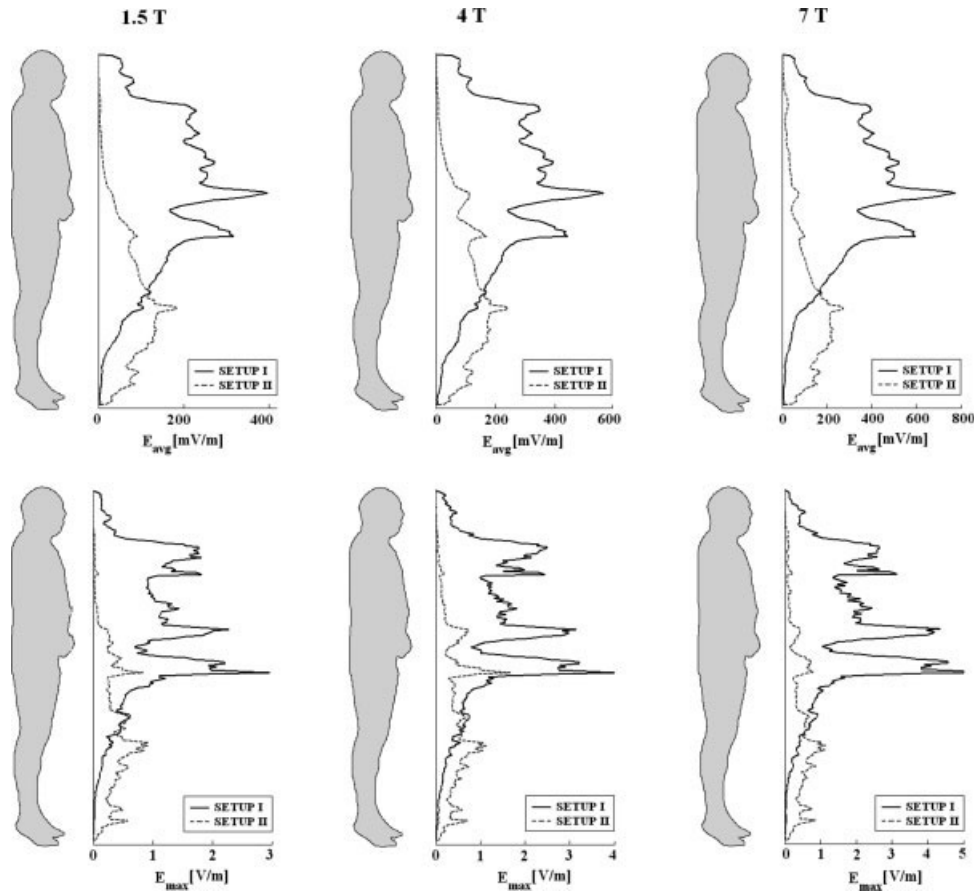


**Figure 8** Comparison of maximum and average electric field for each axial slice versus height of the model worker between setup I and II. The plots are based on motion I around all three superconducting magnets at position A (see Table 3), while very similar profiles are obtained for other assumed body motion–magnet combinations.

as Figs. 6 and 7 illustrate for “setup I.” (Note that the inner bore diameter of the scanner is  $\sim 0.7$  m, which is smaller than that of the main magnet).

By simply lowering the height of the MRI machine by 1 m, as demonstrated in this work, the field induction is shifted from the upper and mid body to the lower body region (i.e., legs and feet), as Figs. 6 and 7 show for “setup II.” With the lowered magnet height, the electric fields induced in the CNS that is located in the head and trunk can be considerably minimized [see Table 5, Figs. 6 and 7 (setup II) and Fig. 9]. According to the simulation results this statement is valid for all combinations of considered motions, positions in front and at the side of the magnets and designated 1.5, 4, and 7 T systems. In particular, as the head of the worker is now at a much higher elevation compared to the bore of the lowered magnet, both the large static magnetic fields and spatial gradients are further away from the head/neck. This results in substantially less electric field expo-

sure to the brain and upper body tissue to fields produced by the main magnet. For instance, lowering the 1.5 T magnet by 1 m in height can lead to an in situ average electric field reduction for white and gray matter by a factor of 53.58 and 51.07 respectively, as Table 5 details. The reduction factors for cerebral spinal fluid (CSF) (i.e., 14.58–29.04) and spine (i.e. 3.47–5.25) in particular are smaller than those of the brain tissue, since the spine (and some CSF contained within) extends from the head/neck down to the lower back/pelvis, and therefore can be closer and thus easily exposed to the gradients of the magnetic field near the bore entrance. To maximize the reduction factors for spine and CSF tissue, one can either lower the magnet by more than 1 m or elevate the healthcare worker near the magnet by implementing a suitable arena/stage as shown in Fig. 13(b). Note also that the ICNIRP limits for instantaneous magnetic flux density in head/trunk and in extremities is 2 and 5T (2), respectively. Therefore,

**Table 4 Quantitative Comparison of Maximum and Average Electric Fields Induced in Central Nervous System of Brook During Motion I at Position A Near the Three Superconducting Magnets**

B (T)	Setup	Spine		CSF		Gray Matter		White Matter	
		$E_{avg}$	$E_{max}$	$E_{avg}$	$E_{max}$	$E_{avg}$	$E_{max}$	$E_{avg}$	$E_{max}$
1.5	I	134.70	680.02	60.98	389.10	52.09	139.33	52.51	121.51
	II	34.73	313.18	2.10	20.80	1.02	3.03	0.98	2.22
4	I	194.77	954.81	87.04	496.30	73.92	214.84	72.22	200.26
	II	56.17	392.55	5.97	61.97	2.58	8.20	2.49	6.01
7	I	253.92	1301.7	94.13	614.09	61.49	217.87	57.41	160.57
	II	48.36	483.26	5.35	24.64	5.29	13.22	5.25	10.71

All electric field values and in units of  $m Vm^{-1}$ . Setup I and II indicate 1.15 and 0.15 m imager elevation respectively. Conductivities of tissues in Table 4 (17, 18) Spine,  $0.02 S m^{-1}$ ; CSF,  $2.00 S m^{-1}$ ; Brain (white matter):  $0.03 S m^{-1}$ ; Brain (gray matter),  $0.03 S m^{-1}$ .

lowering the magnet leads to a smaller magnetic flux density in the head/trunk, and in an increased one within extremities. This is a good trade off as the limit set for extremities is 2.5 times larger than that for head/trunk. According to reduction factor values in Table 5, as the field strength increases, the magnitude of the reduction factor decreases. For example, lowering of the 7T magnet by 1 m, results at best in an average/maximum induced electric field reduction of 11.62/16.48 and 10.93/14.99 for gray and white matter, respectively. Note that for 1.5 and 4 T system the reduction factors are around five and two times larger/better than those of the 7 T system, respectively.

### On the Worker Exposure to Fields Produced by the Gradient Coils

Figure 8 shows that at a conventional magnet height of 1.15 m relative to ground floor, most of the gradient pulsed electric fields are induced near the front surface of the torso (see Fig. 4). As the magnet is lowered by 1 m, the induction region is clearly shifted away from the upper body to the lower legs, as both the coronal, and sagittal body profiles as well as the line graphs illustrate in Figure 10. Interestingly, the exposure of lower leg region is less than one would expect. This is probably because the legs of the worker are somewhat further away from the

end of the gradient set than is the upper body region (i.e., chest and abdominals). Lowering the magnet by more than 1 m in this case would most possibly lead to even less field induction in the upper and mid-body. At this point we can conclude that lowering the imager can significantly reduce the upper and mid-body levels of exposure to both static and low-frequency fields produced by the machine.

### System Setups for Reduced Field Induction

On grounds of CNS exposure during motion in non-uniform static magnetic fields and as magnetic field gradient coils are switched at frequencies of  $\sim 1$  kHz, according to the results of this study, there is a clear benefit of shifting the bore entrance of the imager away from the upper body as far as possible. Therefore moving or standing around a “lowered” imager (i.e.,  $\sim 0.15$  m relative to ground) could cause much less electric field induction in occupational workers compared to conventional elevations (i.e.,  $\sim 1.15$  m relative to ground). Any kneeling/bending down towards the bore entrance of a “lowered” scanner to access the patient near the ground level [see Fig. 13(a)] would decrease the separation of the strong field gradients near the entrance and the upper body region, and subsequently lead to increased field induction in the CNS tissue. To avert healthcare

**Table 5 Reduction Factors (Value Ratio: I/II) of the Field Induction Based on Values in Table 4**

B (T)	Spine		CSF		Gray Matter		White Matter	
	$E_{avg}$	$E_{max}$	$E_{avg}$	$E_{max}$	$E_{avg}$	$E_{max}$	$E_{avg}$	$E_{max}$
1.5	3.88	2.17	29.04	18.70	51.07	45.98	53.58	54.73
4	3.47	2.43	14.58	8.01	28.65	26.20	29.00	33.32
7	5.25	2.69	17.59	24.92	11.62	16.48	10.93	14.99

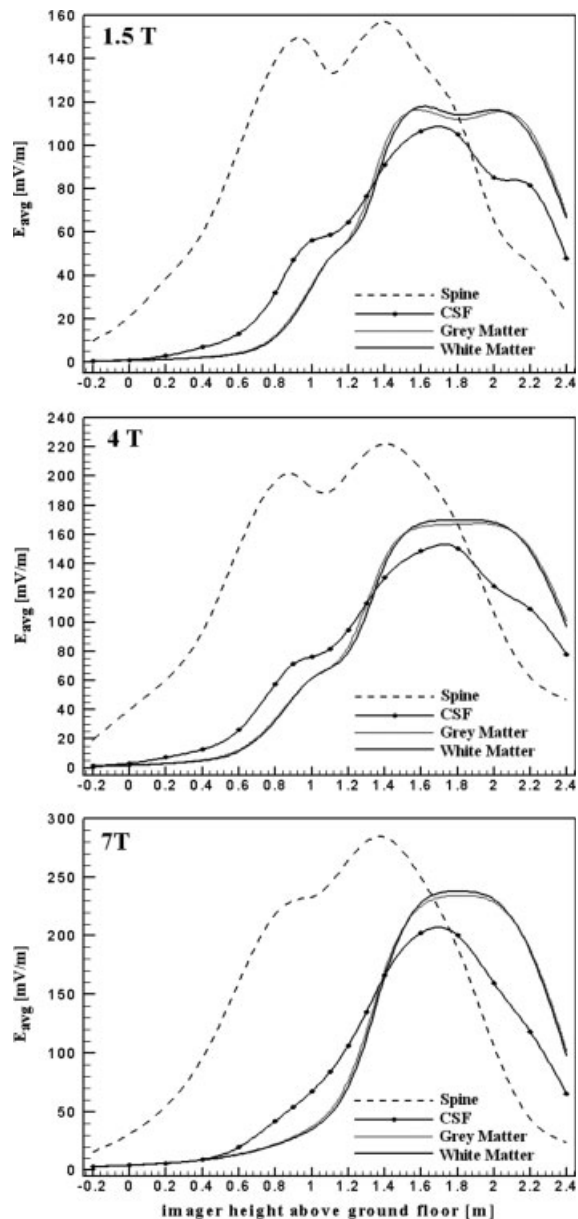


**Figure 9** Average electric field for CNS tissue as a function of magnet height above ground floor.

workers from this undesired action, different MRI system implementations in which the patient table plays an important role are detailed next.

For existing systems it might be difficult and expensive to dig a deep hole in the ground and to situate the MRI scanner therein, as Fig. 4 shows. A more practical and perhaps affordable option would be to construct a dielectric platform (preferably made of wood or plastic) around an existing (or next generation) scanner, which will elevate the occupational worker relative to the bore entrance, as

Fig. 11(a) illustrates. In this particular implementation, the patient table extends well beyond its normal position, so that patient preparation takes places in a

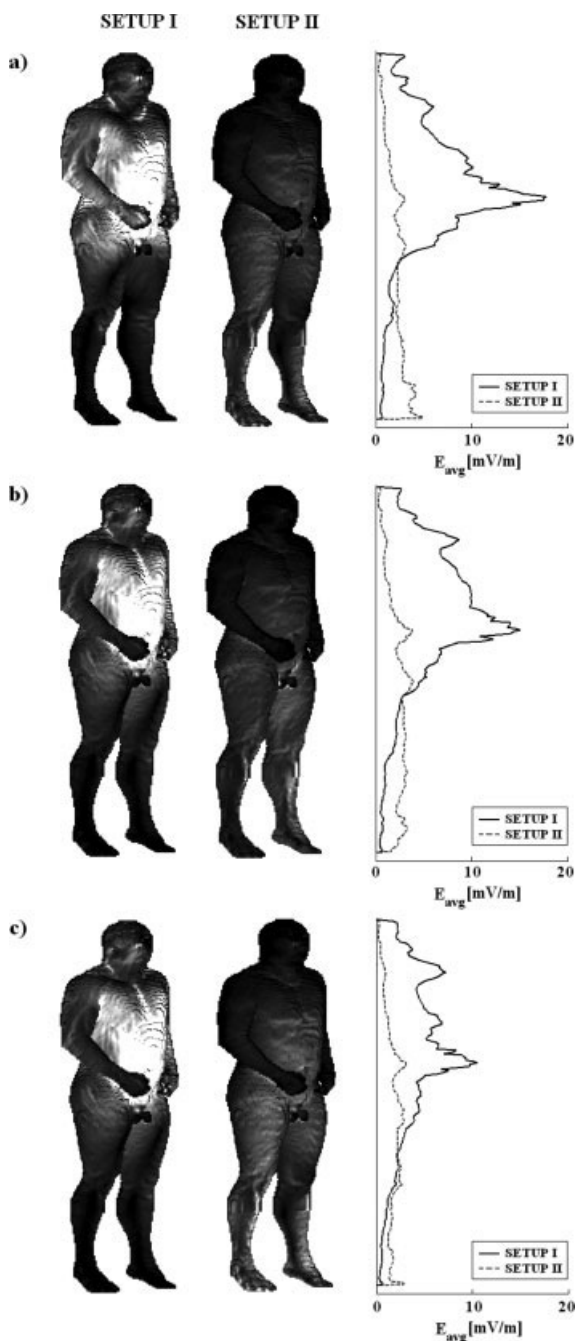


**Figure 10** Electric field distributions on surface of the model worker induced during body exposure to combination of all three gradient coils (each with 1 mT/m central field strength): (a) at position illustrated in Fig. 5(a); (b) at position illustrated in Fig. 5(b); (c) at position illustrated in Fig. 5(c). Also shown on the right are the graphs of average electric field for each axial slice of the model worker versus body height.

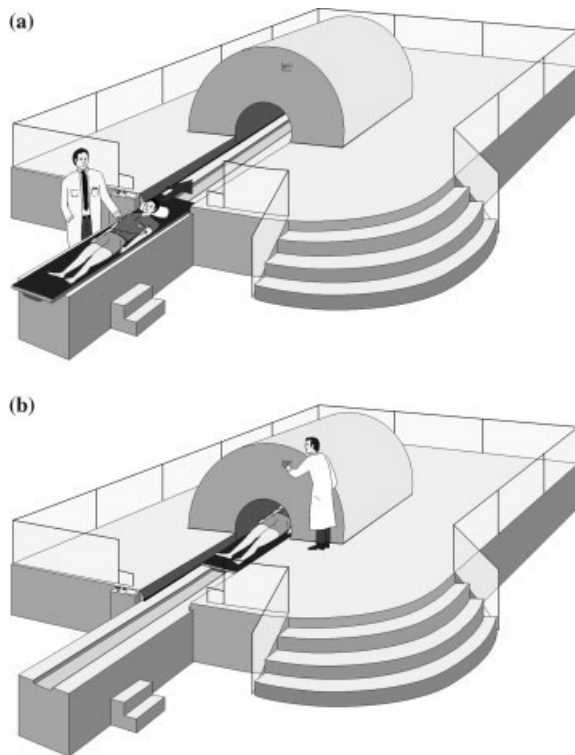


**Figure 11** Worker elevation platform for existing MRI systems: (a) the patient is prepared at a safe location away from strong field gradients of the imager and then moved into the magnet bore for imaging; (b) the occupational worker (here: radiologist) attends the anxious, sedated or intubated patient at a much lower risk of CNS exposure compared to systems with standard imager elevation in respect to the worker (e.g., systems with no added platform).

location away from the strong field gradients that appear near the magnet. While the patient is shifted into the magnet bore at a sensible velocity and the imaging sequence is started, the radiographer (health-care worker) can walk up onto the platform [see Fig. 11(b)]. Compared to the usual implementations, with this new setup, the electric fields/currents induced in the radiographer during standard MRI procedures can be notably minimized (see Table 5). Therefore, this approach could allow one to move faster than fractions of 1 m/s very close to the magnet and yet maintain the induced fields at levels that are several times lower than those induced around a nonlowered imager. We note here that this implementation might not be appropriate for some types of interventional MRI procedures. In conjunction with the lowered imager, it might be viable to include an alarm system that alerts the worker when such bending/kneeling or very fast body movements are unconsciously per-

formed. A portable magnetic field dosimeter that can be worn by operators during normal working shift represents such a system (23). The dosimeter is capable of measuring exposure to magnetic fields, rate of magnetic field change, ambulatory monitoring of instantaneous and cumulative exposure to a wide range of magnetic field frequencies and audibly warns the user of potentially detrimental body actions.

In those instances where the size of the MRI room is not sufficient to implement the extension of the patient table as depicted in Fig. 11(a), it would be certainly feasible to architect a patient table that can be mechanically raised or lowered depending on the need. Fig. 12(a) is an example of this setup, where patient preparation takes place at the usual table height of  $\sim 1.15$  m relative to elevated platform floor, so that strong field gradients near the bore entrance are some distance away from the working/preparation zone. At first, the table would slowly move the patient down into the imaging plane and then eventu-

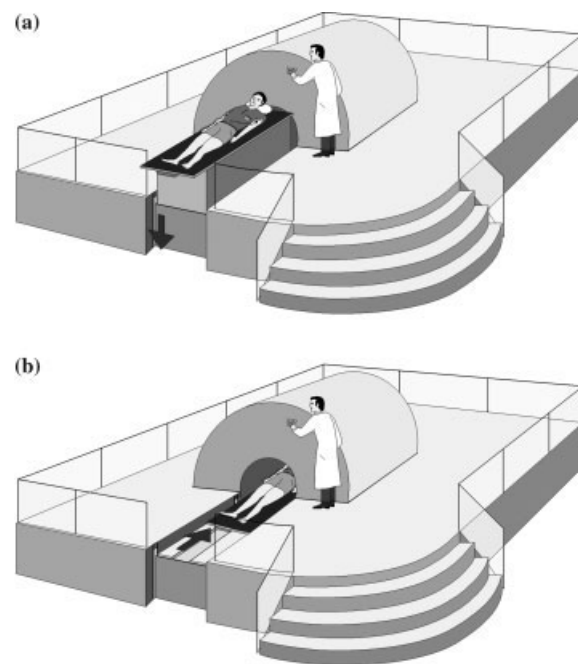


**Figure 12** Worker elevation platform for existing MRI systems: (a) the patient is prepared at a higher table elevation relative to the platform ground (i.e.,  $\sim 1.15$  m) some distance away from the hazardous field gradients produced by the imager. The table is then lowered and the patient is moved into the bore to perform imaging. This implementation benefits MRI rooms that are not large enough to implement patient table mechanism illustrated in Fig. 9; (b) the occupational worker (here: radiologist) attends the patient at a much lesser risk of CNS exposure compared to systems with standard imager elevation in respect to the worker (e.g., systems with no added platform).

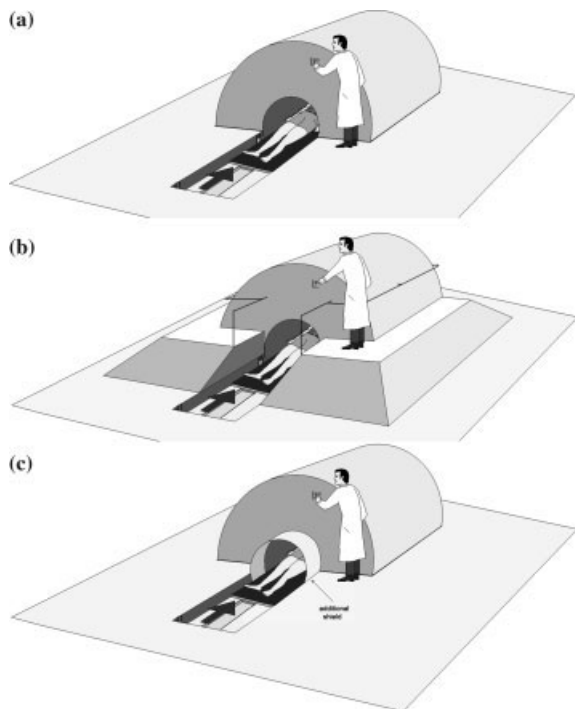


**Figure 13** (a) MRI scanner situated in a ground bed so that the bore opening is as low as possible compared to standard systems. Depending on the design, the patient table can be implemented some distance above the ground, at the ground level or embedded some distance into the ground floor; (b) an extra platform can be constructed that will effectively increase the separation between the upper body of the worker and the imager central axis. This approach can be applied to both MRI setups as illustrated in Figs. 10 and 11 and it could help to further minimize the field induction levels; (c) sketch of additional nonferromagnetic conducting plates at the imager end, which shield low and high frequency fields radially and thus minimize the exposure levels to the body. Note that this does not shield static stray fields.

ally into the magnet bore, as shown in Fig. 12(b). At times it might be necessary to access locations of the scanner that are below the added platform, i.e., during technical inspections, maintenance etc. It is thus prudent to construct the platform in a way that it can be easily taken apart into its constituent building blocks including perhaps an inbuilt wheel mechanism.

If the “magnet height” idea is to be included into the implementation of next generation MRI systems, instead of constructing the elevated platform as illustrated in Figs. 11 and 12, the scanner itself can be lowered and placed into a well premeditated ground opening [see Fig. 13(a)]. Subsequently, the vertically adjustable patient table, as demonstrated in Fig. 12,

can be adopted. This alternative approach would offer substantial mechanical stability to the heavy magnet structure; however it might be difficult to gain access to some parts of the imager if required so for technical reasons. Hence the design of the MRI scanner should be ideally performed with the ground gap in mind.

In scope of “lowered” MRI systems, the exposure of the upper body increases as the vertical distance between the bore entrance and upper body diminishes. Therefore, children and short adults could suffer more CNS field induction than taller subjects would in general. As Fig. 13(b) portrays, this problem can be alleviated by constructing an extra platform in the proximity of the MRI machine that can serve as additional elevation for much safer practice near the scanner. This supplementary elevation can be evidently included into the design of aforementioned platform/ground opening implementations as depicted in Figs. 11–13(a). The employed superconducting magnets (1.5, 4, and 7 T) and gradient coils (longitudinal and transverse) are intended to be typical of currently available cylindrical MRI human/animal systems, but do not cover all products on the market and therefore provide indicative results only. Nonetheless, on grounds of this rather general and intuitive idea, it is strongly believed that the proposed approach can be applied to a wide range of commercially available cylindrical scanners and that in most cases it would be also suitable to other MRI implementations.

Other alternatives for reduced field induction would be to implement next generation main magnets and gradient coil sets with the occupational worker in mind or to design a system which can be retrofitted to existing MRI machines. These solutions would need to take occupational workers into consideration when optimizing the field gradients both radially and axially, particularly in the proximity of the imager where largest field induction is observed. Although these schemes appear quite sensible, their implementation might come at a high financial cost. Like in any other optimization, there could unfortunately be a trade off between the main magnet/gradient coil system performance and the level of anticipated worker exposure. Also, the retrofitting approach might not offer a general solution and hence would need to be specifically tailored for each magnet available on the market. Perhaps the best approach would be to consider either one of these two implementations along with the proposed idea of reducing the magnet height in relation to the occupational worker, since it applies to both existing and future cylindrical MRI systems.

In “lowered” systems where the bore entrance of the imager is much lower than the upper body of the operator, the radio-frequency (RF) fields produced by the volume/surface resonators are also shifted away from the upper to the lower body region, thus minimizing the field exposure of vital body organs/tissues. In existing ultra-short MRI systems, where the gradient set and RF resonators are of similar length as the main superconducting magnet, the cryostat vessel does not always provide sufficient shielding in radial direction near the bore edges at the ends of the scanner. Also, the shorter the main magnet and gradient coils are, the stronger become the accompanied field gradients. Consequently, when ultra-short MRI scanners are lowered in height, the field induction in healthcare worker legs is expected to be somewhat larger than when a longer system is lowered. Yet, for any imager in general (short or long), it might be practical to add extra (multi-layered) cylindrical conducting sheets at the end of the magnet where the patient table is located. The insertion of the removable supplementary radiation shields could effectively reduce the gradient switched and RF-fields in radial direction near the bore entrance, leading to less electric field induction in legs of the occupational worker.

Evidently, it is possible to design MRI systems that reduce worker exposure. Instead of lowering the magnet, one might wish to elevate the magnet in respect to the worker body, in which case the field induction in the head, neck and chest (i.e., vital organs and CNS tissue) would be much stronger than that of lower body for instance (see Fig. 9). In addition, the patients are at a higher risk of injuring themselves if accidentally falling down from the significantly elevated patient table. According to Fig. 9, one would need to elevate the MRI machine by at least 2.5 m in height relative to ground floor to result in noticeable exposure reduction. Clearly, for most MRI systems, this would not be a viable solution.

## CONCLUSIONS

In this numerical study we have demonstrated that decreasing the imager height by at least 1 m can significantly decrease the levels of induced electric fields in the upper body of healthcare workers subject to fields produced by the imager. Compared to other exposure reduction alternatives within the scope of our theoretical exploration, the proposed approach/solution is rather simple to implement for existing and new installations.

## ACKNOWLEDGMENTS

Financial support for this project from The Australian Research Council is gratefully acknowledged. The authors thank the Oxford Magnet Technology for providing the 4T coil pattern.

## REFERENCES

1. Stehling SMK, Turner R. 1998. *Echo-Planar Imaging Theory, Technique and Application*. Springer: New York.
2. International Commission on Non-Ionizing Radiation Protection (ICNIRP). 1998. Guidelines for limiting exposure to time varying electric, magnetic and electromagnetic fields (up to 300 GHz). *Health Phys* 74: 494–522.
3. The Institute of Electrical and Electronics Engineers (IEEE). 2002. C95.6: Standard for Safety Levels with Respect to Human Exposure to Electromagnetic Fields (0–3 kHz), New York.
4. Crozier S, Liu F. 2005. Numerical evaluation of the fields caused by body motion in or near high-field MRI scanners. *Progr Biophys Mol Biol* 87:267–278.
5. National Radiological Protection Board (NRPB). 1993. Restrictions on human exposure to static and time-varying electromagnetic fields and radiation. Documents of the NRPB Vol. 4, No. 5.
6. Hebrank FX. 2000. SAFE model—a new method for predicting peripheral nerve stimulation in MRI. *Proc Int Soc Magn Res Med* 8:2007–2013.
7. Schaefer DJ, Bourland JD, Nyenhuis JA. 2000. Review of patient safety in time-varying gradient fields. *Magn Reson Imag* 12:20–29.
8. Faber SC, Hoffman S, Ruedig C, Reiser M. 2003. MRI-induced stimulation of peripheral nerves: dependency of stimulation threshold on patient positioning. *Magn Reson Imag* 21:715–724.
9. Bourland JD, Nyenhuis JA, Schaefer DJ. 1999. Physiologic effects of intense MR imaging gradient fields. *Neuroimaging Clin N Am* 9:363–377.
10. RR570 report: Assessment of electromagnetic fields around magnetic resonance imaging (MRI) equipment. 2007. Health and Safety Executive. HSE Books.
11. Directive 2004/40/EC of the European parliament and of the council. 2004. *Offic J Eur Union L*. p 159.
12. Hill DLG, Mcleish K, Keevil SF. 2005. Impact of electromagnetic field exposure limits in Europe: is the future of interventional MRI safe? *Acad Radiol* 12:1135–1142.
13. Cheng YCN, Eagan TP, Brown RW, Shvartsman SM, Thopmson MR. 2003. Design of actively shielded main magnets: an improved functional method. *Magma Magn Reson Mater Phys Biol Med* 16:57–67.
14. Trakic A, Liu F, Sanchez LS, Wang H, Crozier S. 2007. Longitudinal gradient coil optimization in pres-

- ence of transient eddy currents. *Magn Reson Med* 57:1119–1130.
15. Crozier S, Forbes KL, Doddrell MD. 1994. The design of transverse gradient coils of restricted length by simulated annealing. *J Magn Reson A* 107:126–128.
  16. Human male voxel phantom BROOK. Brooks Airforce Database. Online: [www.brooks.af.mil/AFRL/HED/hedr/dosimetry.html](http://www.brooks.af.mil/AFRL/HED/hedr/dosimetry.html). Retrieved 2004.
  17. Andreuccetti D, Fossi R, Petrucci C. 2002. Dielectric properties of body tissues. Applied Physics—Italian National Research Council (Florence, Italy). Online: <http://niremf.ifac.cnr.it/tissprop/htmlclie/htmlclie.htm#atsftag>. Retrieved.
  18. Gabriel C, Gabriel S, Corthout E. 1996. The dielectric properties of biological tissues. I. Literature survey. *Phys Med Biol* 41:2231–2249.
  19. Liu F, Zhao HW, Crozier S. 2003. On the induced electric field gradients in the human body for magnetic stimulation by gradient coils in MRI. *IEEE Trans Biomed Eng* 50:804–815.
  20. Forbes LK, Crozier S, Doddrell DM. 1997. Rapid computation of static fields produced by thick circular solenoids. *IEEE Trans Magn* 33:4405–4410.
  21. Liu F, Crozier S, Zhao H, Lawrence B. 2002. Finite-difference time-domain-based studies of MRI pulsed field gradient-induced eddy currents inside the human body. *Concepts Magn Reson* 15:26–36.
  22. Liu F, Crozier S. 2004. Electromagnetic fields inside a lossy, multilayered spherical head phantom excited by MRI coils, models and methods. *Phys Med Biol* 49:1835–1851.
  23. A Magnetic Field Dosimeter—PCT/AU2005/001495. 2007.